Experimental Mechanics (2007) 47:775–787
DOI 10.1007/s11340-007-9042-z

Scanning Electron Microscopy for Quantitative Small and Large Deformation Measurements Part I: SEM Imaging at Magnifications from 200 to 10,000

M.A. Sutton · N. Li · D.C. Joy · A.P. Reynolds · X. Li

Received: 22 August 2006 / Accepted: 30 January 2007 / Published online: 23 March 2007

Abstract A series of baseline displacement measurements have been obtained using 2D Digital Image Correlation (2D-DIC) and images from Scanning Electron Microscopes (SEM). Direct correlation of subsets from a reference image to subsets in a series of uncorrected images is used to identify the presence of non-stationary step-changes in the measured displacements. Using image time integration and recently developed approaches to correct residual drift and spatial distortions in recorded images, results clearly indicate that the corrected SEM images can be used to extract deformations with displacement accuracy of ±0.02 pixels (1 nm at magnification of 10,000) and mean value strain measurements that are consistent with independent estimates and have point-to-point strain variability of $\pm 1.5 \times 10^{-4}$.

Keywords Scanning electron microscopy · Deformation measurements · High and low magnification · 2D digital image correlation · Drift distortion correction · Spatial distortion correction

Introduction

In recent years, the combination of computer vision and Digital Image Correlation (DIC) has been applied to the study of material behavior at the macro-scale: shape, displacement and deformation analysis have been performed successfully using both 2D-DIC [1–4] and 3D-DIC [5–13]. Today, the methodology is one of the preferred optical methods for measurements in experimental mechanics [14].

To perform similar measurements at reduced length scales, 2D-DIC has been applied to analyze images using high-magnification optical systems, such as an optical microscope [15–17]. In this early work, the investigators made 2D deformation measurements over a 0.7×0.7 mm field of view with an accuracy of ±30 nm in the measured displacements, confirming that the method is viable at such length scales.

In contrast to the proven performance of optical methods, the potential for image instability and distortion is considerable for Scanning Electron Microscope (SEM) systems that acquire images through electron beam interaction with the specimen surface. Since a typical modern SEM systems is not closed-loop on e-beam position (i.e., the e-beam position is not a control parameter), positional errors will occur during the scanning process due to a variety of environmental and system variations.

Investigators have noted errors associated with e-beam scanning for lithographic applications [18]. In their studies, where inspection of high-resolution resist structures by SEM imaging was the focus, they have shown that charging of the specimen, and the resulting time-dependent drift variations, have a significant effect on the secondary electron (SE) signal oftentimes used for metrological studies. In another example, Berger et al. [19] reported two error sources when attempting to use SEM-based moiré [20, 21] for measurement of the in-plane displacement field, with the primary error in the measurements being magnification "drift" during imaging (oftentimes associated with specimen charging). The drift variations were estimated to cause errors on the order of ±9% in the measured strains.

M.A. Sutton (✉, SEM member) · N. Li (SEM member) · A.P. Reynolds · X. Li (SEM member)
Department of Mechanical Engineering,
University of South Carolina, Columbia, SC 29208, USA
e-mail: sutton@sc.edu.ph

D.C. Joy
Professor and Director of Nanolithography Facility,
University of Tenessee, Knoxville,
TN 37996-0840, USA

To minimize the positional errors during e-beam scanning, researchers recently modified an existing SEM system to incorporate phase-locked loop control [22]. The control system was designed to provide e-beam position feedback and minimize e-beam positional errors during scanning. Using a 246 nm period, electron-transparent fiducial grid for control purposes, the authors indicated that they reduced positional errors to 1.3 nm for their lithographic application.

In a recent study, the authors proposed an imaging model and a distortion correction methodology to remove both drift and spatial distortions from SEM images [23] for metrology applications. Though image corrections are important for image-based metrology, they are typically not required for those individuals using a modern SEM system for qualitative imaging applications (e.g., metallography, microstructure feature identification, general structure evaluation).

The enclosed work presents results to demonstrate the applicability of the method at a range of SEM magnifications, with Part I focused on evaluating SEM images and Part II directed towards use of SEM images for deformation measurements. In Part I, the stability of images acquired using modern SEM systems is investigated, with emphasis on the deformation measurements extracted from image comparisons. "Scanning Electron Microscopy" provides a brief background for the principles underlying image formation in an SEM. "SEM Pattern Application and Image Evaluation" presents the pattern application process and image evaluation results at 200X, 5,000X and 10,000X for SEM imaging. "Experimental Characterization for Effect of SEM Parameter Variations" presents experimental results describing the effect of variations in SEM imaging parameters on measured full-field displacements. "Discussion" discusses the results.

Scanning Electron Microscopy

Background

Figure 1 shows a schematic of a typical SEM system. A sample is mounted on a mobile stage and electrons emitted by the electron gun are focused through a series of electromagnetic lenses onto the specimen surface. When electrons impinge upon the specimen surface, they interact with the atomic structure. The volume affected by incident electrons is the "interaction volume." The radiation emitted during the interaction includes (a) secondary electrons, (b) back-scattered electrons and (c) additional components such as visible light, auger electrons, and X-rays.

Though all these components are produced simultaneously, they are analyzed independently to generate the type of

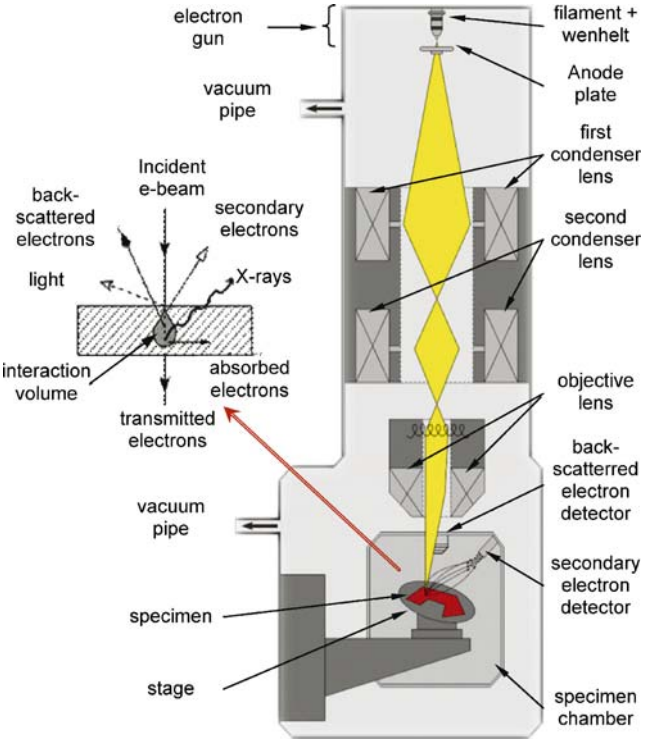

Fig. 1 Schematic of a typical scanning electron microscope and imaging process

information desired. Within all of these components, the secondary electron (SE) and the back-scattered electron (BSE) emissions are of particular interest for our work.

When an incident electron passes through a material, it may transmit a part of its energy to the electron cloud of the specimen atoms, inducing ejection of a secondary electron. Because of their weak energy (<50 eV), secondary electrons are only ejected from the specimen and detected by the SE detector. Since small variations of topography will modify the number of secondary electrons emitted, the information obtained with the SE detector is mainly correlated to the topography of the specimen.

BSE emissions are created when an incident electron is elastically scattered by the atoms of the specimen. The amount of back-scattered electrons collected depends primarily on the charge, hence, the atomic number of the material, rather than the atomic mass. In contrast with the SE signal, the BSE signal represents not only the local topography of the specimen but also information about the local atomic composition of the specimen.

Imaging

As shown in Fig. 2, a digital representation of the specimen is produced by the SEM through a raster process. In a manner that is similar to the approach used to acquire

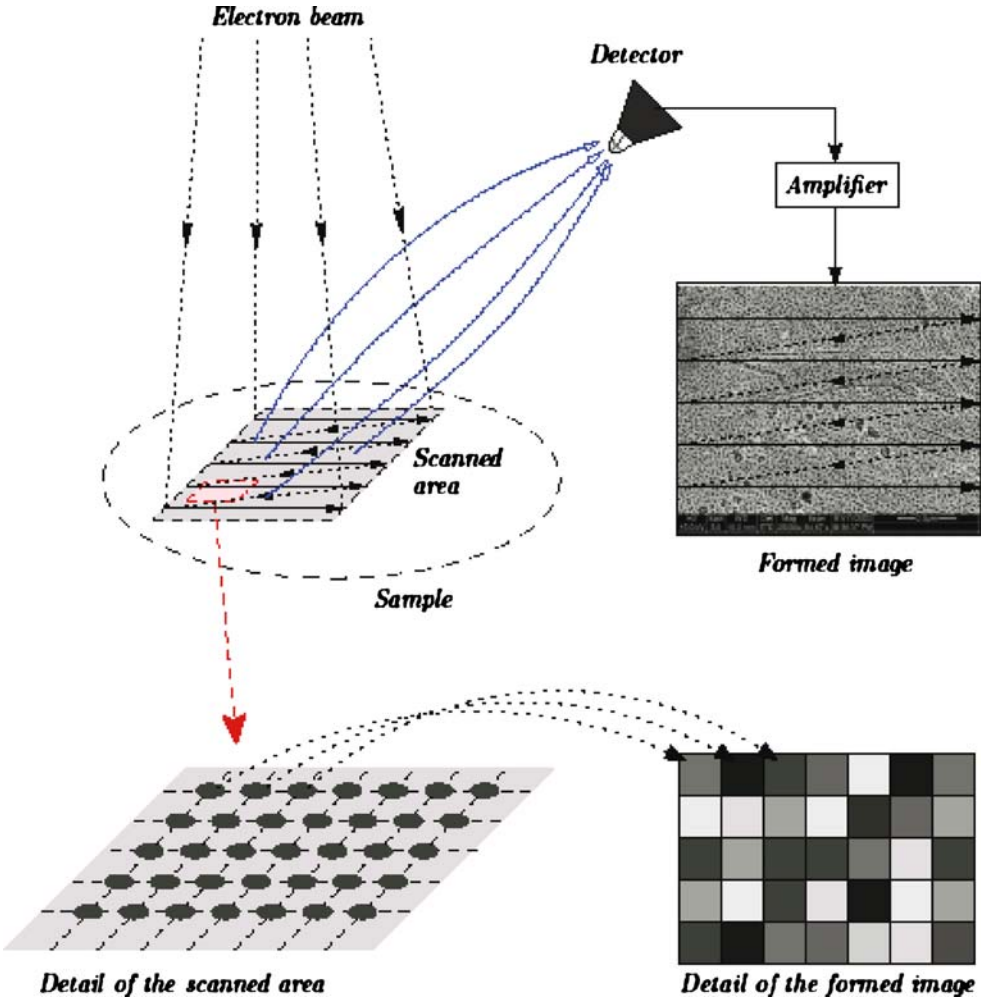

Fig. 2 Schematic of typical image formation process in an SEM. Here, the e-beam is rastering horizontally with a dwell time that is a function of preset scan time to obtain a row of "intensity" data in the digitized image. A delay time between rows is required to reset the e-beam. Either secondary electron detector or back-scattered electron detector is used to record the "intensity" data

images using an early analog optical camera system to either image a specimen or digitize a photograph, the image is acquired through a series of line-scans. In an SEM, the focused e-beam is rastered across the surface of the specimen a total of W times, with the dwell time at each of the H locations selected based upon the preset scan time. The SE (BSE) detector, located within the SEM chamber, records the local emissions of secondary (back-scattered) electrons. The recorded "intensity" data at each (x, y) location is converted into an L-bit integer value.[1] The data from all W×H scan locations is a representation for the L-bit gray-level response of the specimen to the e-beam excitation. Since the specimen surface may have considerable 3D shape variations (topology), and the intensity pattern is a 2D representation of the interaction of the incident e-beam with the specimen's surface, in many cases the process is mathematically considered to be a form of "projection" [24–28].

Figure 3(a) shows an image of a copper penny obtained using SE electrons in our FEI Quanta-200 SEM. As expected, the SE image shows low contrast in relatively flat regions, with high gradients in intensity near the edges. Figure 3(b) shows a BSE image of the same section in the copper penny. The BSE image shows contrast due to both low frequency topology differences and also a higher frequency, high-contrast pattern due to local changes in composition.

Direct comparison of the two images for our gold-on-aluminum specimen shows that the BSE image has much higher contrast than the SE image. The low contrast in the SE image is due to the fact that the topology variations (e.g., surface slopes and curvature) are relatively small and the corresponding spatial frequency of topological changes is relatively low. The high-frequency, randomly varying contrast in the BSE image is primarily due to local variations

[1] In this work, the SEM backscatter detectors typically recorded an image with 8 bits (0–255), though it is possible to record SEM images with additional bits.

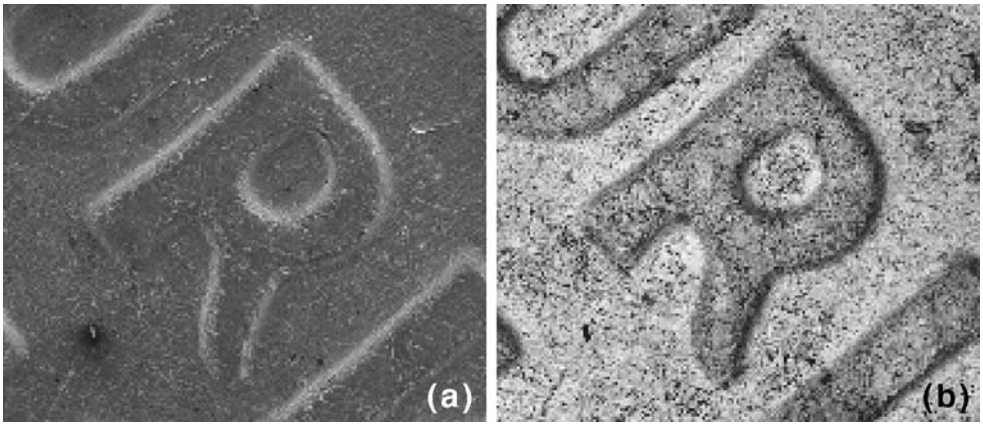

Fig. 3 SEM images acquired of a US penny with (**a**) secondary electron detector and (**b**) back-scattered electron detector

in the composition. It is important to note that in this in stance the BSE image provides a remarkable, high contrast random variation within the intensity pattern that is ideal for image correlation.

SEM Pattern Application and Image Evaluation

Pattern Application

In this study, a miniature specimen is machined from AL2024-T4 sheet with a length of 50 mm, a width of 10 mm and a thickness of 1 mm. To apply a micro-scale pattern to the specimen, the procedure outlined in a previous publication [4] is adapted for this work and briefly described.

First, the specimen surface is polished in water with up to 5 μm grit abrasive paper, ultrasonically cleaned, rinsed in ethanol, dried in nitrogen and stored in a desiccant until coating is performed. The specimen is placed in a coating chamber and the surface is gold-coated by evaporation of gold wire (99.99% purity) from a tungsten boat at a pressure of about 10^{-6} Torr; final thickness of the gold coating is ≈15 nm. To obtain a random gold pattern on the surface, the apparatus shown in Fig. 4 is used, with the temperature of the deionized water vapor held at 95°C for 9 h to complete the coating rearrangement process (the aluminum substrate is not directly heated).

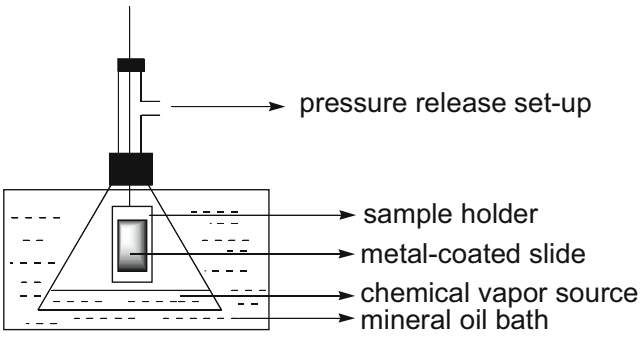

Fig. 4 Schematic of methodology used to convert thin gold film nano-scale random pattern

Figure 5 shows the pattern as imaged at 200X and 5,000X. Since the gold patterned substrate exhibits high contrast in the SEM image and the SEM digitization process has sufficient pixels to resolve the islands when imaging with magnifications ranging from 3,000 to 10,000,[2] subset-based 2D-DIC is appropriate to quantify local motions of similarly patterned specimens.

Single Scan Imaging

Using the specimen and pattern shown in Fig. 5, experiments are performed using three SEM systems: FEI Quanta-200, JEOL JSM-6300 and Hitachi S-4300. In this set of experiments, each image is obtained by performing a single scan of the same specimen. In each experiment, double-sided graphite tape is used to attach the specimen to the metallic SEM translation stage. Liquid graphite is used to increase specimen-to-stage electrical conductivity and minimize specimen charging during the e-beam scanning process. In each experiment, the specimen remained in the same position throughout the imaging process.

Imaging parameters used in each system are given in Table 1. In each case, several consecutive SEM image scans are acquired, with a delay time of 30 s between image scans.

Experimental Results

Using the first image as a reference, 2D digital image correlation is performed on arbitrarily selected images using VIC-2D [14] with a subset size of 43×43, a subset spacing of 5 pixels and a linear subset shape function.

[2] Typically each island must occupy at least 2×2 pixel areas for accurate, subset-based image registration. Since the gold island size ≈300 nm for this specimen, magnifications of 3,000 and 10,000 correspond to ≈2×2 to 6×6 sampling of the specimen pattern. In this case, subset sizes of 15×15 and 41×41 would be reasonable for matching at magnifications of 3,000 and 10,000, respectively.

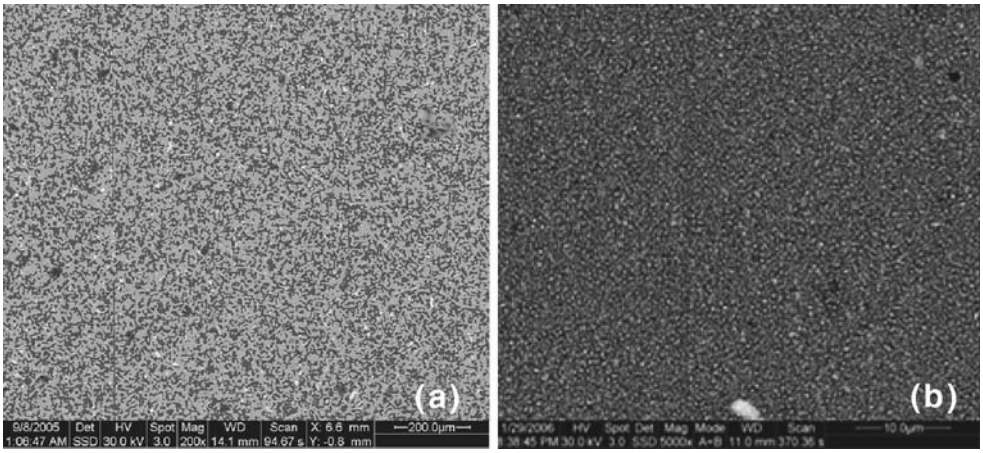

Fig. 5 SEM image of gold-on-aluminum specimen at (**a**) 200X and (**b**) 5,000X

Magnification 200X

FEI Quanta-200 SEM Using the pattern shown in Fig. 5 for 200X magnification, Fig. 6(a) and (b) show the image-correlation measured displacement fields, where the "deformed" image is taken 400 s after the initial image; similar results are observed using the Hitachi SEM system at 200X. The results shown in Fig. 6(a) and (b) indicate that (1) there are random variations in pixel position throughout the image and (2) there are no discernible high gradients or discontinuities in the measured data. Taken together, these observations indicate that, at magnifications on the order of 200X, the SEM imaging system with single scan images provides a reasonable platform for digital image correlation applications [23].

Magnification 5,000X

FEI Quanta-200 SEM Figure 7(a) and (b) shows typical measured displacement fields, where the "deformed" image is taken about 1,600 s after the "reference" image. Figure 7(c) shows a line of vertical (v) displacement data along the vertical direction. As shown in Fig. 7(b) and 7(c), two well-defined *step changes* in the vertical position are measured. Each step change is 0.1–0.2 pixels, corresponding to a vertical shift of 5–10 nm at this magnification.

It is noted that Fig. 7 demonstrates that the vertical shifts are primarily a function of the vertical position, y, being constant along the scan direction. Since y corresponds to the direction perpendicular to each scan line, the step change implies that a sudden change in e-beam position has occurred prior to initiating further horizontal scans, with the pixel distance between step changes ≈270 pixels in this case.

JEOL JSM-6300 SEM To determine whether similar sharp changes in position occur in other SEM systems, an older SEM (manufactured in 1992) in a separate laboratory is also employed to obtain a series of images of the same specimen at 5,000X. Figure 8 shows typical measured horizontal (u) and vertical (v) displacement fields, where the delay time between the images is 300 s. As expected, a step change in the vertical displacement is clearly visible,

Table 1 Parameters for single scan imaging

Imaging properties	FEI Quanta-200	FEI Quanta-200	JEOL JSM-6300	Hitachi S-4300
Magnification	200X	5,000X	5,000X	5,000X
Electron detector	BSE	BSE	BSE	BSE
Detector mode	Compositional	Compositional	Compositional	Compositional
Working distance (mm)	14	14	13	12.7
Vacuum mode	High vacuum	High vacuum	High vacuum	High vacuum
Accelerating voltage (kV)	30	30	10	20
E-beam spot size	3 (4 nm)	3 (4 nm)	13 (6 nm)	5 nm
Dwell time (μs)	100	100	153	100
Image size	1,024×884	1,024×884	1,024×768	1,280×960
Object magnification	1.25 μm/pixel	50 nm/pixel	50 nm/pixel	40 nm/pixel
Recording pixel shape	Square	Square	Square	Square
Image quantization (bits)	8	8	8	8

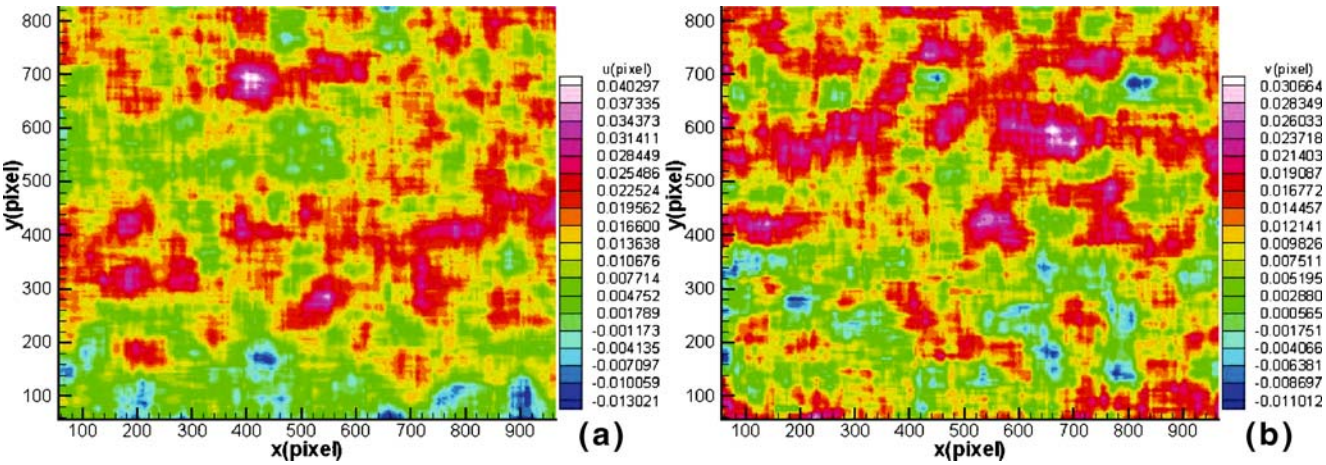

Fig. 6 (**a**) Horizontal and (**b**) vertical displacement fields at 200X using FEI Quanta-200 SEM. Dwell time is 100 μs. Random variations are observed without discernible high gradients

with the magnitude of the shift ranging from 0.73 to 0.95 pixels, corresponding to a positional shift of 36.4–47.5 nm.

Figure 9 shows the measured u- and v-displacement field using an image acquired 600 s after the "reference" image. Here, the data shows that the u-field and v-field also may incur shifts, along with a secondary noise component that is sinusoidal in the horizontal (scan) direction.

Hitachi S-4300 SEM A nearly identical experiment is performed on a relatively modern Hitachi S-4300 SEM in a different laboratory to test the limitations in the technology and to determine whether similar sub-pixel step changes occur on a nearly state-of-the-art system.

Figure 10 shows measured horizontal (u) and vertical (v) displacement fields, where the time delay between the "reference" and "deformed" image is 900 s. The results confirm that a step change is clearly measured in the v-displacement field. In this case, the measured shift is ≈0.19 pixels or 7.5 nm at this magnification.

Discussion of Experimental Findings

Based on the consistency of the observations across three laboratories and three different SEM systems, the results presented above are believed to be generic to single-scan images in SEM systems.[3] Thus, it is expected that similar SEM imaging systems will have similar image shifts.

As shown in Fig. 8, the position of the measured step changes in the u- and v-displacement fields *do not occur at the same location in all images*. Since the spatial location of the step change varies across a series of images, this phenomenon *cannot* be interpreted as a spatial distortion field and cannot be removed using recently developed non-parametric methods for spatial distortion extraction [13, 23]. Furthermore, since the current approach for removing drift distortion assumes that it is relatively smooth and a C^1 function in time, the current analytic approach for removing noise *cannot be used effectively to remove the effects of such random step changes in position from the data*.

Based on our experimental data, the older JEOL JSM-6300 SEM has (a) larger shifts than the other two SEMs, especially in the direction perpendicular to the scan line, and (b) additional sinusoidal disturbances (wavelength of 90–105 pixels corresponding to a temporal oscillation of 73–62 Hz for the u-displacement field), indicating that the older system is unlikely to be viable for image-based metrology.

Experimental Characterization of Effect of SEM Parameter Variations

Since the presence of the measured image shifts will affect the accuracy of image extraction methods for deformation measurements, several SEM imaging parameters are varied to quantify their effect on the measured displacement field and to identify an approach to minimize the image shift.[4] Throughout this effort, all imaging is performed using the FEI Quanta-200 SEM in high vacuum mode with the imaging parameters given in Table 1.

[3] Another SEM, using a cold field emission gun (FEG), within Oak Ridge National Laboratory was used in September, 2005. When the images were compared using 2D-DIC, position step changes were measured throughout the imaging process.

[4] Several suggestions were provided by Dr. John Caola and Dr. Richard S. Van Luvender Jr. from FEI.

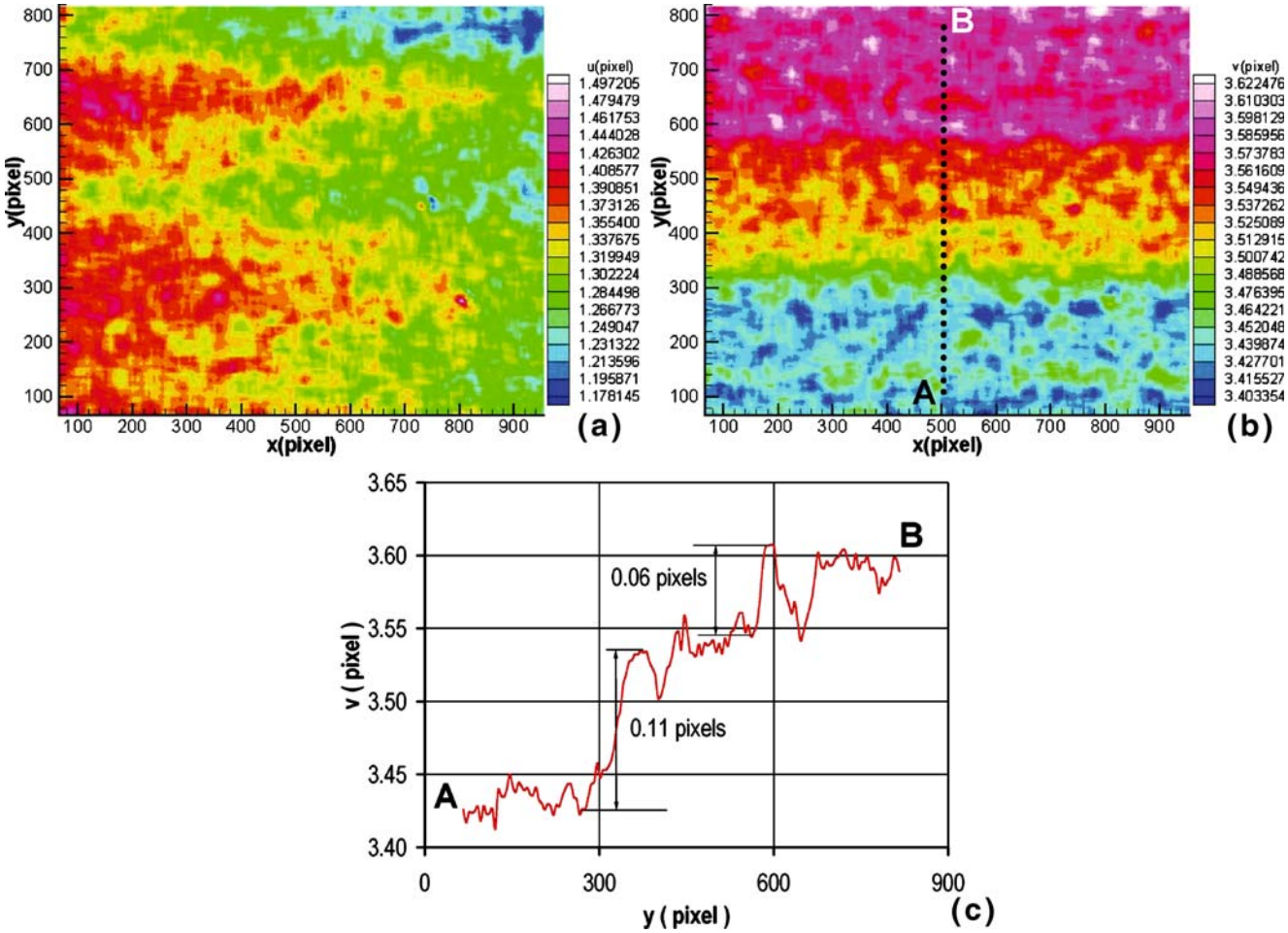

Fig. 7 (**a**) Horizontal and (**b**) vertical displacements fields at 5,000X using FEI Quanta-200 SEM. Dwell time is 100 μs. Shifts ≈0.1 pixels (5 nm). (**c**) Line plot of step changes in v-displacement field

Digitized Image Size

In this study, the digitized image size is increased by a factor of two to 2,048×1,768 while retaining the same object field of view at 5,000X. The delay time between the "reference" and the "deformed" images is 400 s. Figure 11 shows the measured horizontal and vertical displacement fields, confirming that an image shift is still present. The measurements indicate that the image shift in the vertical direction is 0.4 pixels (10 nm) which is nearly twice the physical size measured previously (the in-plane magnification factor for 1,024×768 images is on the order of 50 nm/

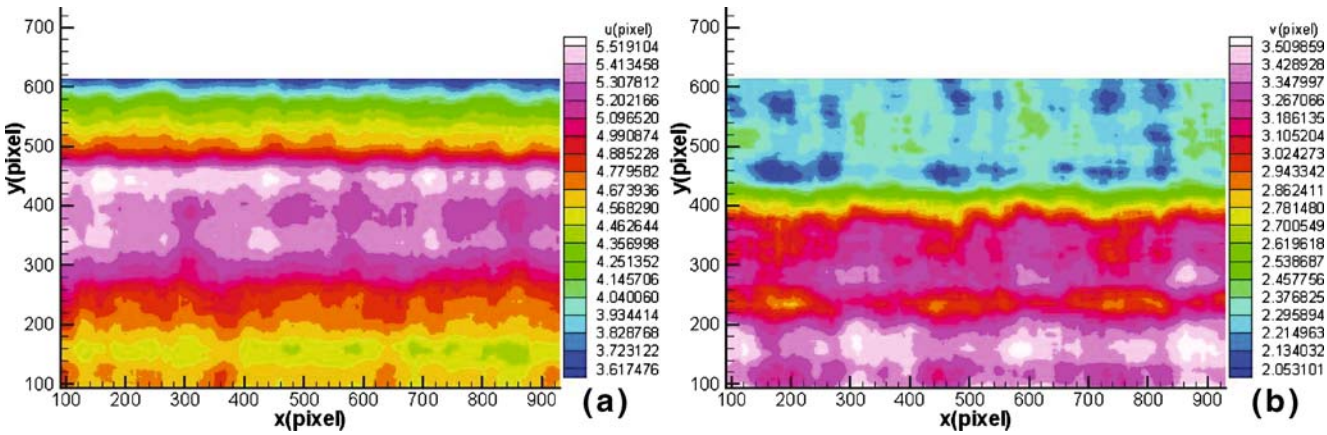

Fig. 8 (**a**) u- and (**b**) v-displacement fields at 5,000X using JEOL JSM-6300 SEM. Vertical and horizontal shifts ≈0.8 pixels (40 nm)

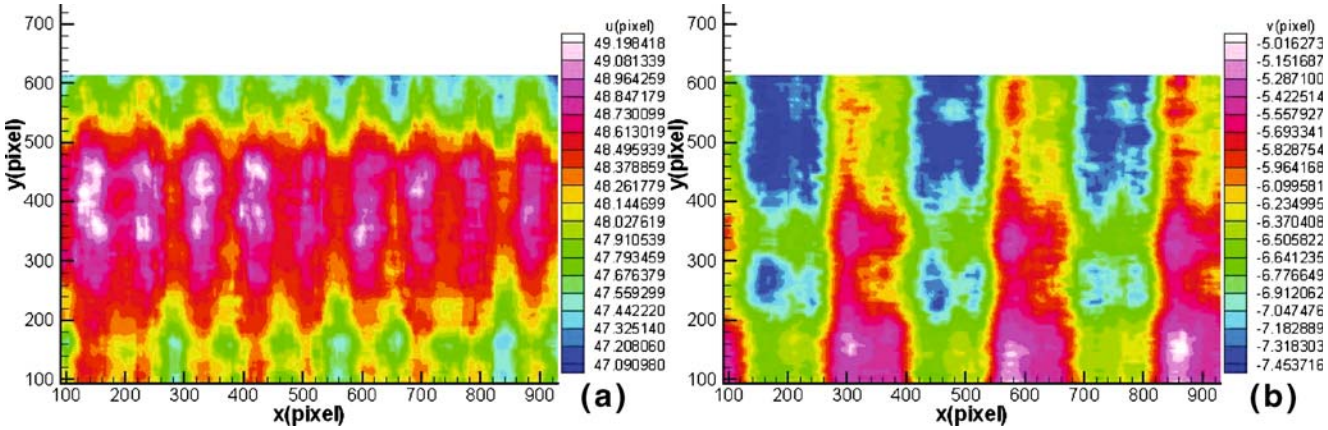

Fig. 9 Additional (**a**) u- and (**b**) v-displacement fields measured on the JEOL JSM-6300 SEM showing both step changes and sinusoidal noise

pixel so that each 0.1 pixel step change is on the order of 5 nm). The pixel distance between step changes is approximately 260 pixels in this case.

Dwell Time

In this study, the dwell time is decreased to 50 μs and then 25 μs, resulting in two- and four-fold decreases in total scan time, while retaining a 2,048×1,768 digitized image size; the time between the "reference" and the "deformed" images is 800 and 100 s, respectively. Typical results are shown in Fig. 12, confirming that the measured displacement fields indicate the presence of shifts on the order of 0.4 pixels (10 nm) and that the presence and magnitude of image shifts are not affected by dwell time. However, the results do indicate that the shorter dwell time introduces larger random noise in the images and hence increases variability in the measured displacement field.

Working Distance

While keeping the dwell time at the same value, a series of experimental studies are performed by changing the working distance from 10.2 to 6.2 mm while keeping the same field of view (magnification factor of 10,000X). As shown in Fig. 13, image shifts were present at both working distances. However, the size of the step change in the horizontal and vertical displacement components decreased with working distance by factors of 1.3 and 3.0, respectively.

Assuming that angular variability, $\Delta\ominus$, is independent of working distance, the observed reduction in vertical displacement shift with decreasing working distance (for a fixed scan area) should be on the order of (1–6.2/10.2 mm) or ≈40%, which is in reasonable agreement with the estimated 23% reduction for the horizontal motion. However, additional experiments would be required to firmly establish the relationship.

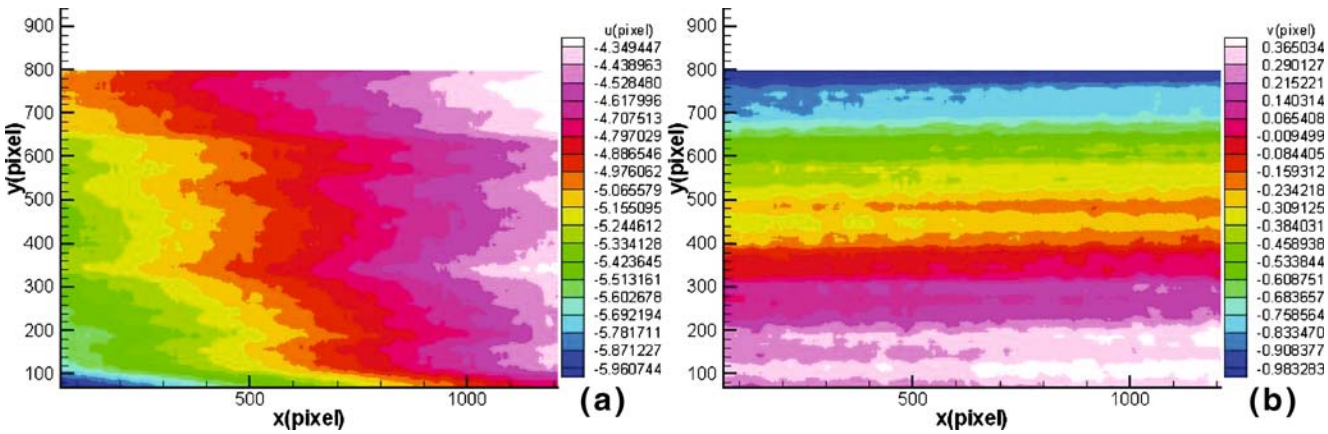

Fig. 10 (**a**) u- and (**b**) v-displacement fields measured on the Hitachi S-4300 SEM. Step changes in vertical displacement are ≈0.19 pixels (7.5 nm)

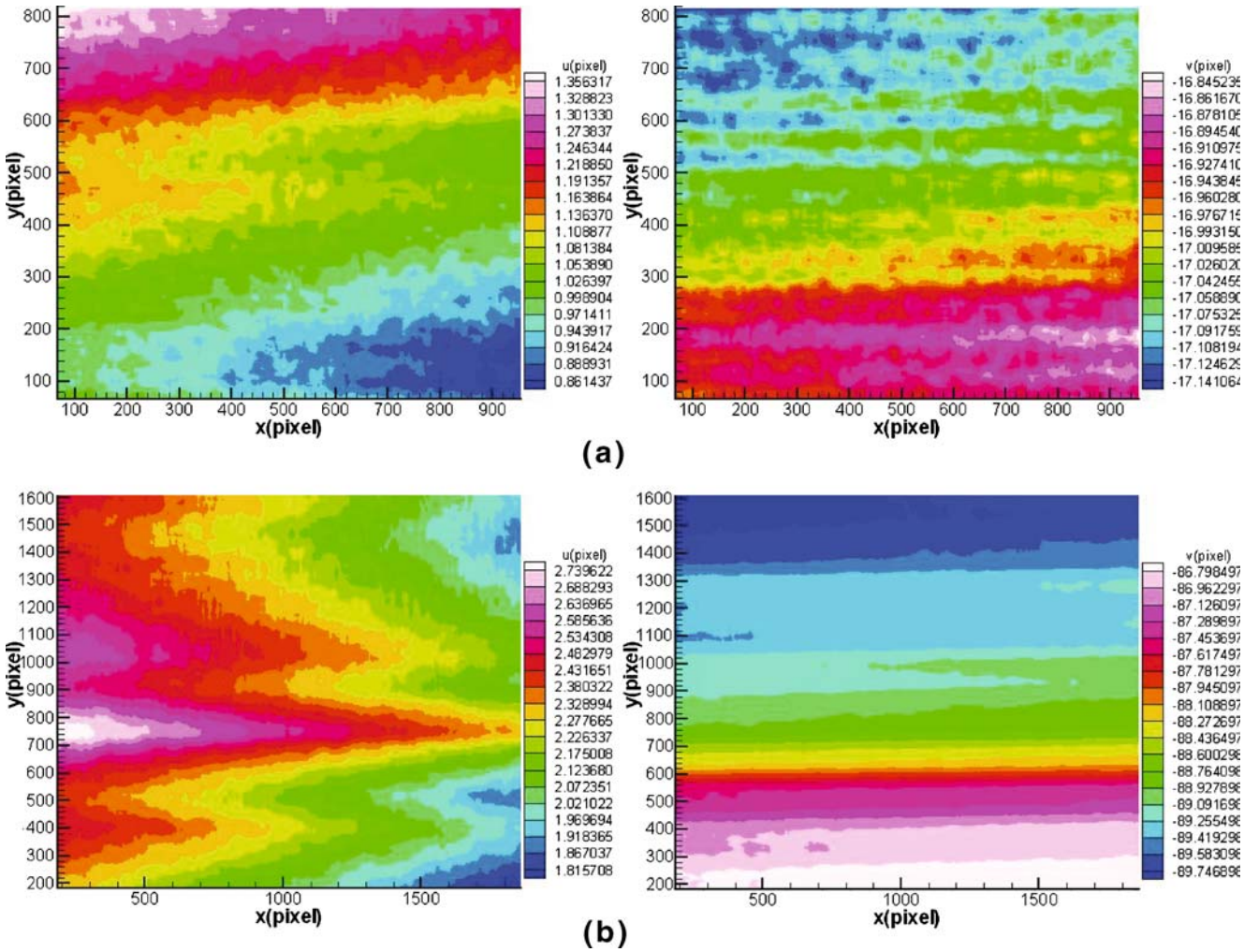

Fig. 11 Step changes in horizontal and vertical displacement fields for (**a**) 1,024×884 and (**b**) 2,048×1,768 image sizes using FEI Quanta-200 SEM and 100 μs dwell time. Measured step changes in v- displacements are on the order of 0.4 pixels (10 nm) for 2,048×1,768 image size

Integration Time

Defining the integration process as the average of a sequence of images by the formula

$$r_i = \frac{(n-1)r_{i-1} + g_i}{n}, i = 1, \cdots, n; n = 1, 2, 4, 8, 16, \cdots \quad (1)$$

where g_i is the signal of each scan, r_i is the signal in the image memory after the ith scan, n is the integration time to be selected.

Integrated images were obtained using (a) the same total scan time for all images, (b) the remaining SEM parameters shown in Table 1 and (c) a spatial resolution of 1,024×884. As shown in Fig. 14, increasing the total number of scans from 1 to 8 indicates that the integration process eliminated the step changes in both directions.

Discussion

As discussed in the previous sections, baseline studies in an SEM at magnification of 5,000X have shown that small step changes in position do occur, indicating that the SEM scanning process introduces small shifts in image position.

With regard to the step-change measurements, detailed experimental studies using several SEM systems indicate that, when imaging a specimen for 1–2 h in an SEM, (a) the magnitude of the step changes and the overall trends in the measured fields are relatively unchanged, and (b) the spatial position of the measured step change in position varies from image to image in a random manner. This observation was confirmed by performing image integration process without increasing the overall scan time and demonstrating that the step changes can be removed. Given the fact that such step changes will introduce large strains errors, the

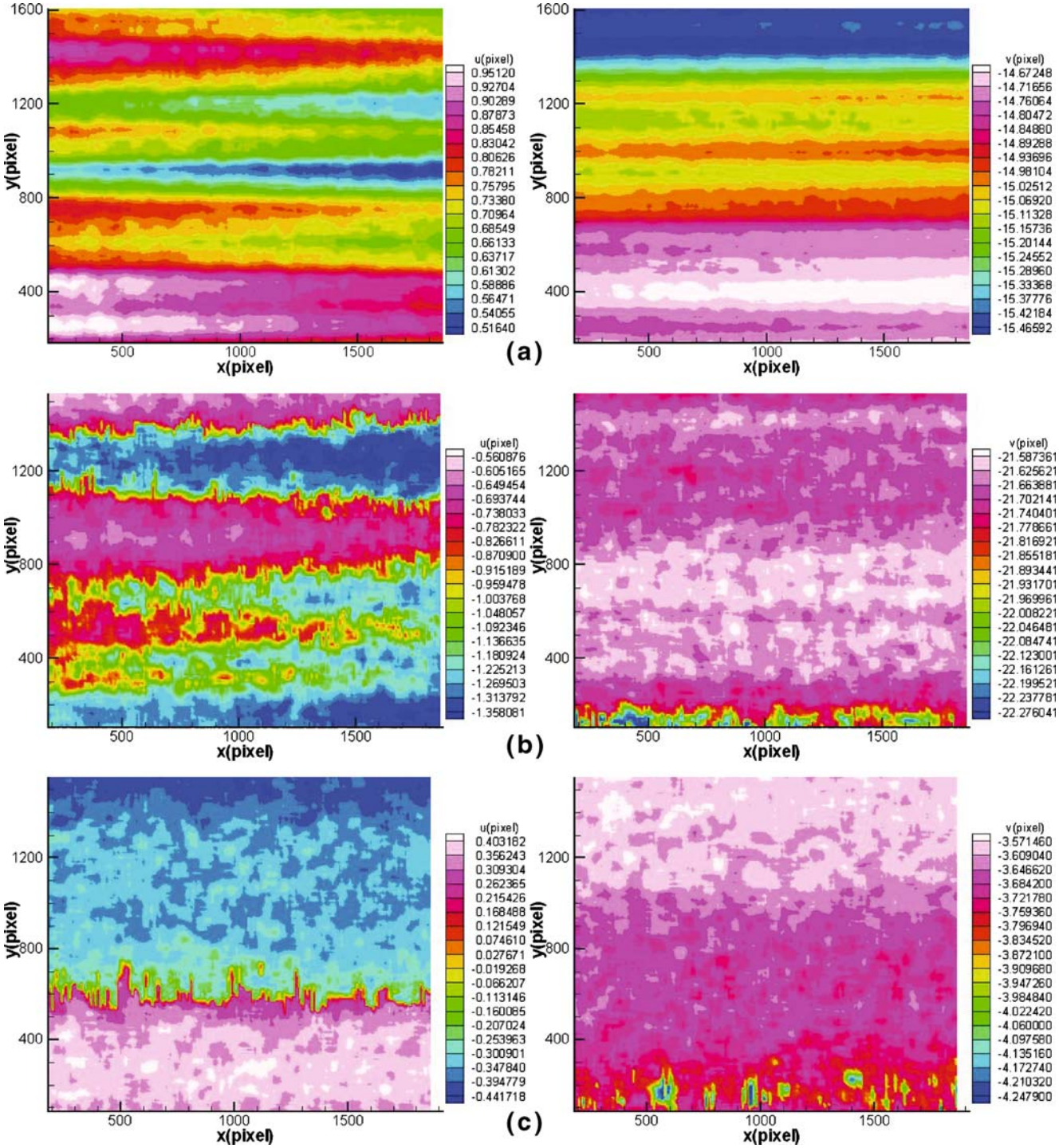

Fig. 12 Using FEI Quanta-200 SEM step changes in horizontal and vertical displacement fields for dwell times (**a**) 100, (**b**) 50 and (**c**) 25 μs with 2,048×1,768 image size. Maximum step change is ≈0.4 pixels (10 nm)

integration process is essential to ensure accurate strain/deformation measurements when performing image-based deformation extraction procedures.

Though not observable using digital image correlation at low magnification,[5] a wide range of experimental studies using several modern SEM systems indicates that image shifts observed in our studies have a magnitude O(10^{-8} m).

[5] If one assumes that the same dimensional step change would occur at any magnification, then a 10 nm step change would correspond to an error of 0.008 pixels at a magnification of 200X. Consistent with the results shown in Fig. 6, this deviation would not be readily visible in the computed distortion fields at 200X since it is below the noise level for these cases.

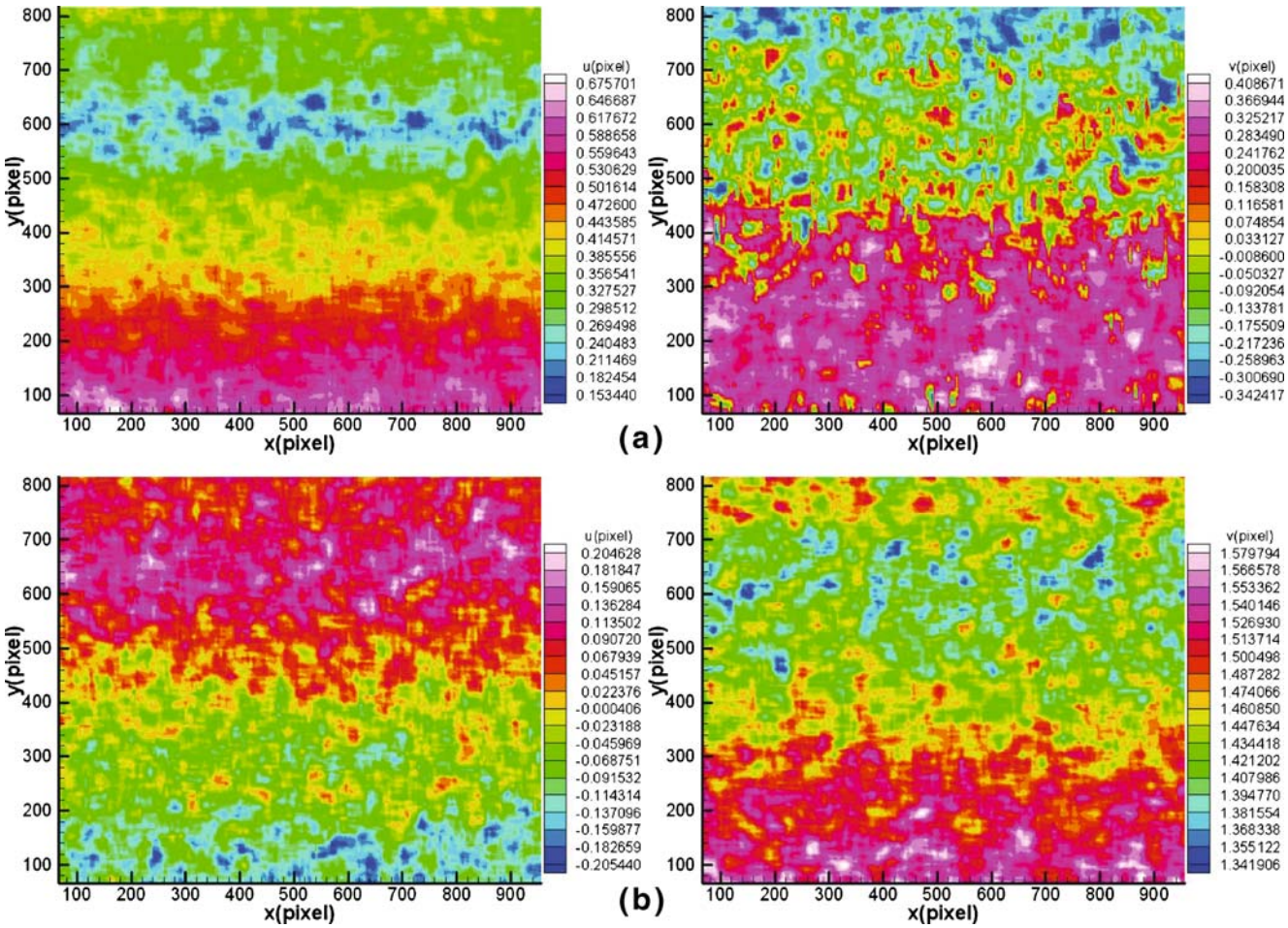

Fig. 13 Horizontal and vertical displacement fields from FEI Quanta-200 SEM using 1,024×884 image size with dwell time of 40 μs (frame time 37.87 s) and field of view of 25.6 μm×22.1 μm for (**a**) working distance of 6.2 mm and (**b**) working distance of 10.2 mm. Image shifts are observed in both cases, with reductions in magnitude with reduced working distance. Similar results obtained with dwell times of 20 and 80 μs

For example, at 5,000X the measured step change of 0.5 pixels corresponds to ≈10 nm when converted to metric distance, with the steepest gradient measured for the v-displacement field. Thus, image integration sets the lower bound on spatial resolution in the integrated image to ≈1 pixel (20 nm) at 5,000X. Since the subset size used to extract deformation measurements is much larger than this lower bound, the integration process will have minimal effect on the subset-based displacement measurement process.

As shown in Table 1, all images in this study were obtained using the BSE *compositional signal*. A typical BSE detector has two half-disk shaped components, A and B, to record independent readings for each pixel. The *compositional signal* is obtained by summing the signals from A and B and is oftentimes designated A+B.[6] The A+B signal is known to be relatively shape-invariant and is useful when the specimen is not ideally polished.

Conclusions

Detailed imaging studies with multiple SEM systems confirm that image shifts occur at random positions during the imaging process, demonstrating that the image errors are a generic feature of the SEM imaging systems employed in this study. Due to the indeterminate (random) nature of the image shifts, their presence will reduce the accuracy of image-based methods for deformation measurement, especially at higher image magnification.

The effect of image shifts on the resulting strain field can be minimized (for the range of magnifications under consideration) through implementation of an image integration procedure that combines image data from multiple scans without increasing overall scan time.

[6] The topographic signal, which is the difference in the signals from A and B, A–B, is to be affected by surface topography on the specimen. Though not used in these studies, it may be worthwhile to perform an experiment using the A–B signal to define each image.

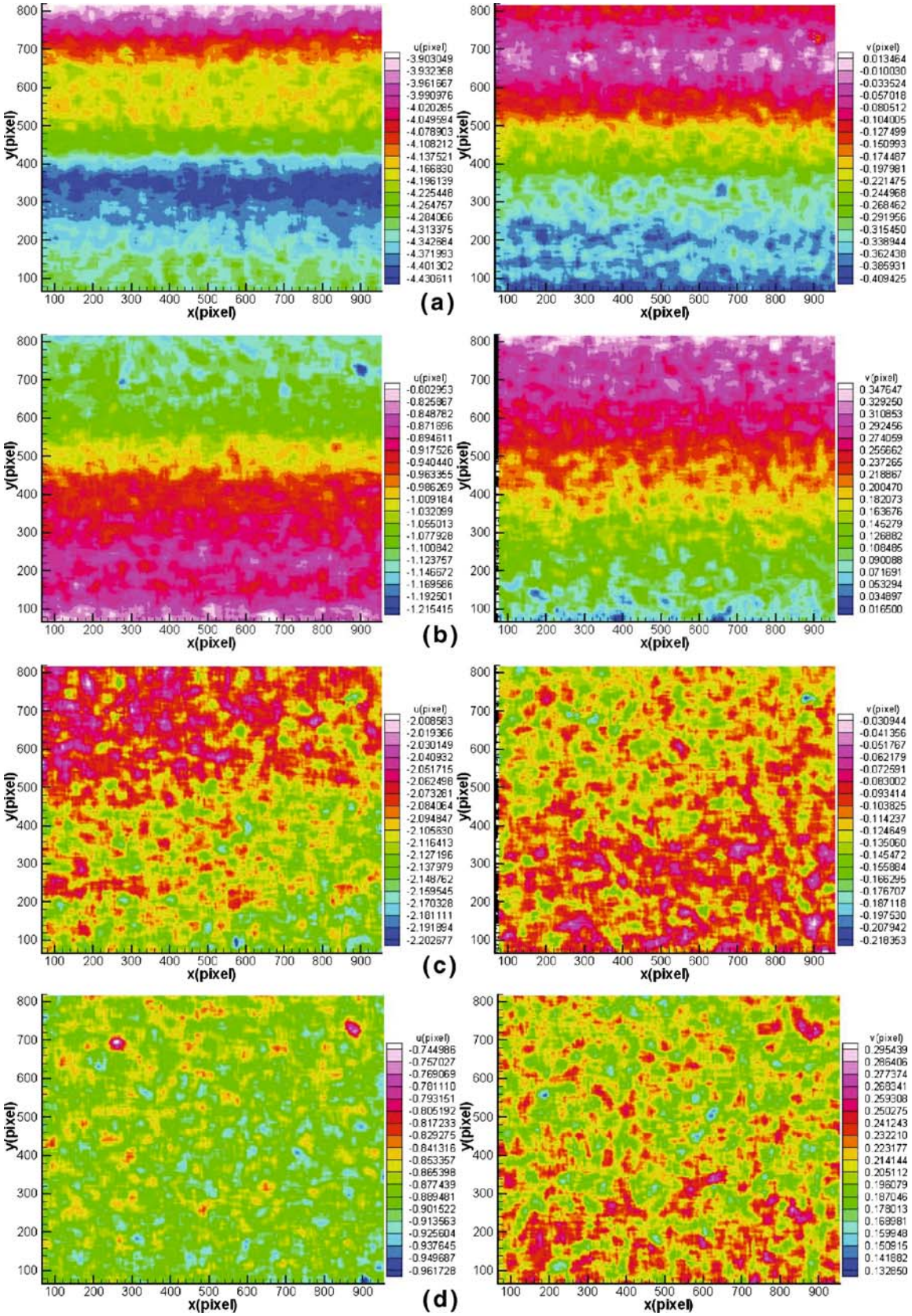

Fig. 14 Horizontal and vertical displacement fields of 1,024×884 image size for (**a**) 80 μs dwell time with one scan, (**b**) 40 μs dwell time with integration over two scans, (**c**) 20 μs dwell time with four scans and (**d**) 10 μs dwell time with eight scans. The total time to acquire an image is same but the step-changes disappear with increasing integration time (e.g. increased number of scans that are combined.)

References

1. Peters WH, Ranson WF(1982) Digital imaging techniques in experimental stress analysis. Opt Eng 21(3):427–432.
2. McNeill SR, Sutton MA, Wolters WJ, Peters WH, Ranson WF (1983) Determination of displacements using an improved digital correlation method. Image Vis Comput 1(3):1333–1339.
3. Chu TC, Ranson WF, Sutton MA, Peters WH (1985) Application of digital image correlation techniques to experimental mechanics. Exp Mech 25(3):232–244.
4. Sutton MA, Cheng M, Peters WH, Chao YJ, McNeill SR (1986) Application of an optimized digital correlation method to planar deformation analysis. Image Vis Comput 4(3):143–153.
5. Khan-Jetter ZL, Chu TC (1990) Three-dimensional displacement measurements using digital image correlation and photogrammic analysis. Exp Mech 30(1):10–16.
6. Luo PF, Chao YJ, Sutton MA (1994) Application of stereo vision to 3D deformation analysis in fracture mechanics. Opt Eng 33 (3):981–990.
7. Helm JD, McNeill SR, Sutton MA (1996) Improved 3D image correlation for surface displacement measurement. Opt Eng 35 (7):1911–1920.
8. Orteu JJ, Garric V, Devy M (1997) Camera calibration for 3D reconstruction: application to the measure of 3D deformations on sheet metal parts. In; European symposium on lasers, optics and vision in manufacturing. Munich, Germany, pp 252–263. (August).
9. Synnergren P, Sjodahl M (1999) A stereoscopic digital speckle photography system for 3D displacement field measurements. Opt Lasers Eng 31(6):425–443.
10. K. Galanulis, Hofmann A (1999) Determination of forming limit diagrams using an optical measurement system. In: 7th international conference on sheet metal. Erlangen, Germany, pp 245–252. (September).
11. Sutton MA, McNeill SR, Helm JD, Schreier HW (2000) Computer vision applied to shape and deformation measurement. In: International conference on trends in optical nondestructive testing and inspection. Lugano, Switzerland, pp 571–589. (May).
12. D. Garcia (December 2001) Mesure de formes et de champs de déplacements tridimensionnels par stéréo-corrélation d'images. PhD thesis, Institut National Polytechnique de Toulouse, France.
13. Schreier HW, Garcia D, Sutton MA (2004) Advances in light microscope stereo vision. Exp Mech 44(3):278–288.
14. Correlated Solutions Inc.; VIC-2D and VIC-3D; 952 Sunset Blvd., W. Columbia, SC 29252; http://www.correlatedsolutions.com.
15. Sutton MA, Chae TL, Turner JL, Bruck HA (1990) Development of computer vision methodology for the analysis of surface deformations in magnified images. In: MiCon90: advances in video technology for micro-structural control, George F. Van Der Voort, Ed., ASTM STP 1094:109–132.
16. Mazza E, Danuser G, Dual J (1996) Light optical measurements in microbars with nanometer resolution. Microsyst Technol 2 (2):83–91.
17. Mitchell HL, Kniest HT, Won-Jin O (1999) Digital photogrammetry and microscope photographs. Photogramm Rec 16 (94):695–704.
18. Grella EL, Luciani L, Gentili M, Baciocchi M, Figliomeni M, Mastrogiacomo L, Maggiora R, Leonard Q, Cerrina F, Molino M, Powderly D (1993) Metrology of high-resolution resist structures on insulating substrates. J Vac Sci Technol, B, Microelectron Nanometer Struct 11(6):2456–2462.
19. Berger JR, Drexler ES, Read DT (1998) Error analysis and thermal expansion measurement with electron-beam moiré. Exp Mech 38(3):167–171.
20. Dally JW, Read RT (1993) Electron-beam moiré. Exp Mech 33 (2):270–277.
21. Read DT, Dally JW (1996) Theory of electron-beam moiré. J Res Natl Inst Stand Technol 101(1):47–61.
22. Hastings JT, Zhang F, Smith HI (2003) Nanometer level stitching in raster scanning electron beam lithography using spatial phase locking. J Vac Sci Technol, B, Microelectron Nanometer Struct 21 (6):2650–2656.
23. Sutton MA, Li N, Garcia D, Cornille N, Orteu JJ, McNeill SR, Schreier HW, Li XD (2006) Metrology in SEM: theoretical developments and experimental validation. Meas Sci Technol 17:2613–2622.
24. Hemmleb M, Albertz J, Schubert M, Gleichmann A, Köhler JM (July 1996) Digital microphotogrammetry with the scanning electron microscope. XVIII ISPRS Congress, Commission V. Vienna, Austria.
25. Lacey AJ, Thacker NA, Yates RB (1996) Surface approximation from industrial SEM images. In: British Machine Vision Conference (BMVC'96) 725–734.
26. Agrawal M, Harwood D, Duraiswami R, Davis L, Luther P (2000) Three-dimensional ultrastructure from transmission electron microscope tilt series. In: 2nd Indian conference on vision, graphics and image processing (ICVGIP 2000). Bangalore, India.
27. Vignon F, Le Besnerais G, Boivin D, Pouchou JL, Quan L (June, 2001) 3D reconstruction from scanning electron microscopy using stereovision and self-calibration. Physics in Signal and Image Processing. Marseille, France.
28. Sinram O, Ritter M, Kleindiek S, Schertel A, Hohenberg H, Albertz J (2002) Calibration of an SEM, using a nano positioning tilting table and a microscopic calibration pyramid. In: ISPRS Commission V Symposium. Corfu, Greece, pp 210–215.